Van Wyk, J. J., Svoboda, M. E., & Underwood, L. E. (1980) *J. Clin. Endocrinol. Metab. 50*, 206-208.
White, M. F., Häring, H. U., Kasuga, M., & Kahn, C. R. (1984) *J. Biol. Chem. 259*, 255-264.
White, M. F., Maron, R., & Kahn, C. R. (1985) *Nature 318*, 183-186.
White, M. F., Shoelson, S. E., Keutmann, H., & Kahn, R. (1988) *J. Biol. Chem. 263*, 2969-2980.
Williams, P. F., & Turtle, J. R. (1979) *Biochim. Biophys. Acta 579*, 367-374.
Yarden, Y., & Ullrich, A. (1988) *Annu. Rev. Biochem. 57*, 443-47.

X-ray Absorption Spectroscopic Studies of the High-Spin Iron(II) Active Site of Isopenicillin N Synthase: Evidence for Fe–S Interaction in the Enzyme–Substrate Complex†

Robert A. Scott,* Shengke Wang, and Marly K. Eidsness

Departments of Chemistry and Biochemistry and Center for Metalloenzyme Studies, University of Georgia, Athens, Georgia 30602

Aidas Kriauciunas, Charles A. Frolik, and Victor J. Chen*

Lilly Research Laboratories, Indianapolis, Indiana 46285

Received December 18, 1991; Revised Manuscript Received February 28, 1992

ABSTRACT: Isopenicillin N synthase from *Cephalosporium acremonium* (IPNS; M_r 38.4K) is an Fe^{2+}-requiring enzyme which catalyzes the oxidative conversion of (L-α-amino-δ-adipoyl)-L-cysteinyl-D-valine (ACV) to isopenicillin N, with concomitant reduction of O_2 to $2H_2O$. Chemical and spectroscopic data have suggested that catalysis proceeds via an enzyme complex of ACV bound to the iron through its cysteinyl thiolate [Baldwin, J. E., & Abraham, E. P. (1988) *Nat. Prod. Rep. 5*, 129-145; Chen, V. J., Orville, A. M., Harpel, M. R., Frolik, C. A., Surerus, K. K., Münck, E., & Lipscomb, J. D. (1989) *J. Biol. Chem. 264*, 21677-21681; Ming, L.-J., Que, L., Jr., Kriauciunas, A., Frolik, C. A., & Chen, V. J. (1991) *Biochemistry 30*, 11653-11659]. Here we have employed the technique of Fe K-edge extended X-ray absorption fine structure (EXAFS) to characterize the iron site and to seek direct evidence for or against the formation of an Fe–S interaction upon ACV binding. Our data collected in the absence of substrate and O_2 are consistent with the iron center of IPNS being coordinated by only (N,O)-containing ligands in an approximately octahedral arrangement and with an average Fe–(N,O) distance of 2.15 ± 0.02 Å. Upon anaerobic binding of ACV, the iron coordination environment changes considerably, and the associated Fe EXAFS cannot be adequately simulated without incorporating an Fe–S interaction at 2.34 ± 0.02 Å along with four or five Fe–(N,O) interactions at 2.15 ± 0.02 Å. Although these data cannot rule out incorporation of an endogenous thiolate from the protein coincident with ACV binding, evidence presented in the following paper indicates that the thiolate ligand originates from ACV [Orville, A. M., Chen, V. J., Kriauciunas, A., Harpel, M. R., Fox, B. G., Münck, E., & Lipscomb, J. D. (1992) *Biochemistry* (following paper in this issue)]. Multiple-scattering analysis of the EXAFS data shows that two or three of the Fe–(N,O) interactions are likely due to histidyl imidazole ligation, both in the presence and in the absence of ACV.

Isopenicillin N synthase (IPNS;[1] M_r 38.4K) is a mononuclear Fe^{2+}-dependent enzyme (Chen et al., 1989) which catalyzes the formation of isopenicillin N from (L-α-amino-δ-adipoyl)-L-cysteinyl-D-valine (ACV); concomitantly, one O_2 is reduced to $2H_2O$ (White et al., 1982; Baldwin & Abraham, 1988; Scheme I), in classic oxidase stoichiometry. To date, IPNS is the only oxidase known among a growing number of mononuclear non-heme Fe^{2+}-dependent enzymes. More typically, the enzymes in this class catalyze oxygenase chemistry, wherein one or both atoms of O_2 are incorporated into substrates (Ingraham & Meyer, 1985). A variety of activation mechanisms have been proposed for these enzymes, all invoking activation of O_2 through interaction with the enzyme-bound iron center.

The roles of O_2 and iron in the IPNS reaction are less well-defined. Since the double ring closure of ACV is a 4-electron oxidation process, O_2 may serve as an electron acceptor analogous to its role in cytochrome *c* oxidase (Chan et al., 1988). Alternatively, O_2 may be activated at the iron center to become a reagent which is essential for generating certain reactive substrate intermediates during the ring closure reaction. Pursuant to this hypothesis is a mechanism for IPNS

† XAS studies at the University of Georgia are supported by National Institutes of Health Grant GM-42025 to R.A.S.

* Correspondence can be addressed to either of these authors. The address for V.J.C. is Lilly Research Laboratories, MC797, Lilly Corporate Center, Indianapolis, IN 46285.

[1] Abbreviations: ACV, (L-α-amino-δ-adipoyl)-L-cysteinyl-D-valine; EXAFS, extended X-ray absorption fine structure; IPNS, isopenicillin N synthase; MOPS, 3-(*N*-morpholino)propanesulfonic acid; XAS, X-ray absorption spectroscopy.

0006-2960/92/0431-4596$03.00/0

Scheme I

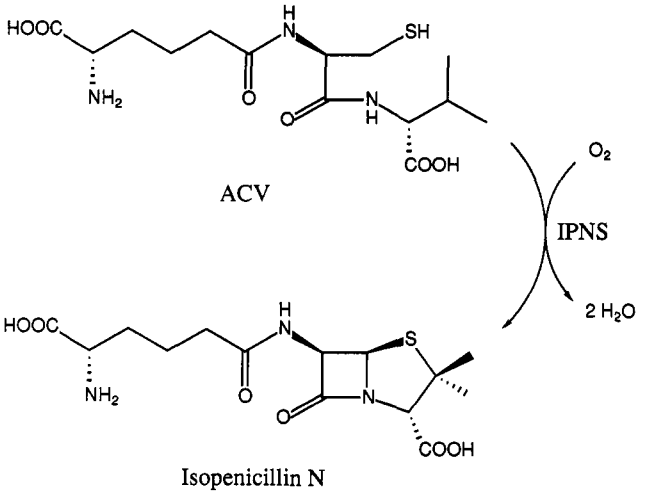

Isopenicillin N

put forward by Baldwin and his co-workers [for a review, see Baldwin and Abraham (1988)] which suggests that the stereospecific closures of the β-lactam and thiazolidine rings proceed in a stepwise fashion and evolve from a complex consisting of both O_2 and ACV coordinated to the iron. Coordination of ACV via its cysteinyl thiolate was suggested to facilitate the transfer of two electrons from the closure of the β-lactam to O_2, resulting in the cleavage of the O–O bond and the formation of a high-valent iron–oxo species, RS—Fe(IV)=O, still containing substrate–thiolate ligation. This iron–oxo species is proposed to play a pivotal role in oxidative formation of the thiazolidine ring. This mechanism has received support in several studies wherein IPNS has been shown to catalyze oxygenation of substrate analogues bearing susceptible acceptor groups in place of the valinyl side chain of ACV. Nevertheless, from these studies, no direct evidence can be derived for the critical Fe–O_2 or Fe–ACV interactions.

We have initiated a series of investigations using different spectroscopic techniques to elucidate the coordination chemistry at the iron site of IPNS. The binding of ACV to IPNS induces a number of spectral perturbations that are consistent with the coordination of an electron-rich atom to the metal center. These include the following: (a) significant decreases in the value of the Mössbauer isomer shift parameter, implying increased covalency of the iron center, upon formation of the IPNS·ACV and IPNS·ACV·NO complexes (Chen et al., 1989; Orville et al., 1992); (b) the appearance of a pink color and a visible absorption spectrum indicative of S → iron charge transfer in IPNS·ACV·NO (Chen et al., 1989; Orville et al., 1992); and (c) the appearance of an absorption band at 385 nm characteristic of S → Cu^{2+} charge transfer upon adding ACV to Cu^{2+}-reconstituted IPNS (Ming et al., 1990, 1991). While all of these changes may be explained by coordination of the ACV thiolate, the ligation of an endogenous cysteinyl thiolate or a tyrosine phenolate cannot be rigorously excluded. Other data from magnetic resonance studies of Fe^{2+}-IPNS and its Cu^{2+}- and Co^{2+}-reconstituted analogues have provided evidence suggesting that the endogenous ligands include the side chains of two or three histidines and an aspartic acid residue (Ming et al., 1991; Jiang et al., 1991). Although addition of ACV resulted in considerable spectral perturbations, no resonances in the ^{1}H-NMR spectrum are readily assignable to the β-CH_2 protons of an enzyme-bound metal-binding cysteinyl residue, leaving the nature of the Fe–ACV interaction in doubt.

We have now employed the technique of X-ray absorption spectroscopy to examine the coordination of the iron center in IPNS with the specific aim of seeking direct evidence for or against the formation of an Fe–S interaction upon ACV binding. We find that the high-spin Fe^{2+} in the free enzyme is in a nearly octahedral coordination environment consisting of only (N,O)-containing ligands. ACV binding under anaerobic conditions unambiguously results in the incorporation of a sulfur atom into the Fe^{2+} coordination sphere. In the following paper (Orville et al., 1992), we provide evidence that the source of this coordinated thiolate is ACV rather than either of the two endogenous cysteines of IPNS.

Experimental Procedures

The IPNS protein used in this work was the recombinant apoenzyme of *Cephalosporium acremonium* purified and analyzed according to Kriauciunas et al. (1991). Reconstituting this apoIPNS with 1 molar equiv of Fe^{2+} gave a preparation of holoenzyme exhibiting a specific activity of 9 units/mg when assayed by initial-rate oxygen consumption in the presence of 5 mM ACV, 5 mM ascorbate, and 0.1 M MOPS, pH 7.1 (Kriauciunas et al., 1991). For XAS studies, holoIPNS was obtained by carefully infusing 1 equiv of Fe^{2+} under anaerobic conditions into a solution of apoenzyme previously dialyzed into a buffer solution containing 30% glycerol and 0.1 M MOPS, pH 7.1.

Two sets (A and B) of IPNS samples were prepared for XAS, each consisting of one sample of holoenzyme and one sample of IPNS·ACV complex which was generated by anaerobic addition of a solution of holoenzyme to solid ACV lyophilized from a pH 7.1 solution. ACV concentrations were chosen on the basis of its K_d value of 18 mM, estimated by Mössbauer titration (Orville et al., 1992), predicting 91% saturation at 0.19 M ACV. The ACV concentrations in the IPNS·ACV samples were estimated to be 0.10–0.19 M (set A) and 0.19 M (set B).

The spectroscopic experiments were conducted as "blind" experiments: XAS data were collected and analyzed on coded samples of both sets, A and B, before the identity of the samples was revealed. XAS data collection was performed at both the Stanford Synchrotron Radiation Laboratory (SSRL) and the National Synchrotron Light Source (NSLS) at Brookhaven National Laboratory. Data reduction was performed using the XFPAK software package developed by one of us (R.A.S.) as described previously (Scott, 1985). Details of the data collection and reduction are summarized in Table I.

The high-resolution X-ray absorption edge data (collected only on samples from set B) were analyzed to obtain integrated 1s → 3d peak intensities. Normalized fluorescence data in the 7090–7120-eV region were fit using nonlinear least squares to the sum of a second-order polynomial, an arctangent function, and a Gaussian to represent the 1s → 3d peak (at ~7112 eV). In the case of the IPNS·ACV sample, a second Gaussian was required to fit a shoulder in the edge at ~7118 eV. The Gaussian fits to the 1s → 3d peaks were numerically integrated and the results expressed in units of electronvolts (eV).

Curve-fitting analyses of the EXAFS data used scattering functions calculated by the FEFF program (v3.25) (Rehr et al., 1991). The first-shell analyses used Fourier-filtered EXAFS data including only the major FT peak in each Fourier transform (cf. Figures 2c and 3c). Crude estimates of Fe–(N,O) and Fe–S distances were obtained from XFPAK fits to empirical scattering parameters obtained from model compounds (Scott, 1985), and then FEFF was used to calculate Fe–N and Fe–S scattering parameters for those distances.[2]

Table I: X-ray Absorption Spectroscopic Data Collection and Reduction for IPNS Samples

	edges	EXAFS (A/B)[a]
SR facility	SSRL	NSLS/SSRL
beam line	VII-3	X10C/VII-3
monochromator crystal	Si[220]	Si[111]/Si[220]
energy resolution (eV)	~2	?/~4
detection method	fluorescence	fluorescence
detector type	13-element solid-state array[b]	13-element solid-state array[b]
scan length (min)	15	30/21
scans in average	2	12/15
metal concentration (mM)	2.3	2.6/2.3
temperature (K)	10	12/10
energy standard	Fe foil (1st inflection)	Fe foil (1st inflection)
energy calibration (eV)	7111.2	7111.2
E_0 (eV)	7130	7130
preedge background energy range (eV) (polynomial order)	7200–7510 (2)[c]	7200–7825 (2)[c]
spline background energy range (eV) (polynomial order)	7200–7510 (2)	7155–7330 (2) 7330–7530 (3) 7530–7826 (3)

[a] Where different for sample sets A and B, values are separated by a slant (/). [b] At SSRL, the 13-element Ge detector was maintained by the SSRL Biotechnology Program. At NSLS, the 13-element Ge detector was courtesy of G. N. George, Exxon Research and Engineering (Cramer et al., 1988). [c] The background was calculated from fitting this (EXAFS) region, and then a constant was subtracted so that the background matched the data just before the edge (Scott, 1985).

In all FEFF calculations, the amplitude reduction factor was set to 0.9, the Debye–Waller factor (σ^2) was set to zero, the coordination numbers for central and scattering atoms were left as 1, and the muffin-tin potential overlap was set to 1.0 (no overlap). All other parameters were defaulted to values recommended by the FEFF authors (Rehr et al., 1991). The resulting FEFF scattering parameters were ported to XFPAK and used in curve-fitting optimizations that varied only absorber–scatterer distance (R_{as}) and Debye-Waller factor (σ_{as}^2). Tests of such FEFF parameters on a series of model compounds determined that a ΔE_0 of +10 eV was required (i.e., 10 eV must be added to the calculated phase functions) to match these parameters to our arbitrary selection of E_0 = 7130 eV used in extracting the experimental EXAFS. These tests also confirmed that the FEFF parameters give very good representations of Fe EXAFS modulations down to 7145 eV and yield bond distances to an accuracy better than ±0.02 Å.

To estimate the outer-shell Fe EXAFS contribution from potential histidyl imidazole ligation to the IPNS Fe site, a multiple-scattering analysis was performed using the EXCURV86 software (Strange et al., 1987). For first-shell Fe–N and Fe–S and second-shell single-scattering Fe–C EXAFS contributions, calculated FEFF scattering parameters were used as "templates" to match EXCURV86 calculated scattering parameters to the FEFF parameters. Scatterer phase shifts were calculated in EXCURV86 and fit to the FEFF templates, yielding bond distances within ±0.01 Å of the FEFF distances and ΔE_0 = 32 eV. Using these adjusted scattering parameters, the first-shell contributions were fit to a first-shell Fourier filter varying R_{as} and σ_{as}^2 and then fixed for fits to the raw EXAFS data varying the second-shell Fe–C and third-shell Fe–(C,N) imidazole contributions, including multiple scattering for the third shell. Possible numbers of histidine imidazole ligands were selected from fits that generated physically reasonable Debye-Waller factors for the outer shells, as determined by test fits on structurally characterized imidazole-containing model compounds.

[2] Although scattering functions were generated for Fe–N and Fe–S only, other tests indicate that identical results would be obtained with Fe–O and Fe–Cl functions, respectively. Thus, we do not claim to distinguish between Fe–N and –O or between Fe–S and –Cl. The uncertainty in EXAFS-derived Fe–(N,O) coordination numbers is ±1 for the fits in Table II (Scott, 1985).

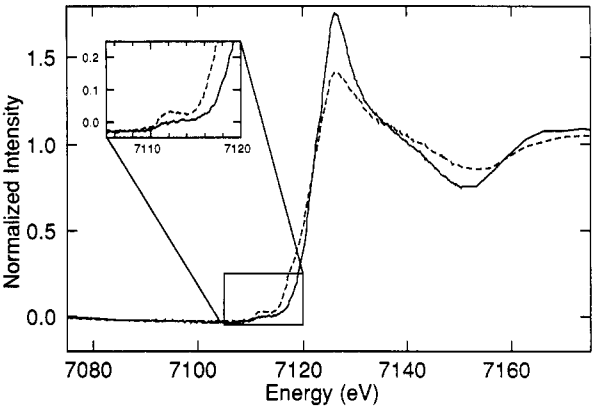

FIGURE 1: Fe K X-ray absorption edge spectra for IPNS (—) and the IPNS·ACV complex (- - -), both from sample set B. The data in the region of the 1s → 3d transition are expanded in the inset.

RESULTS

X-ray absorption spectroscopic analysis of the coded samples within each set of IPNS samples (±ACV) indicated a series of consistent differences. The most obvious differences were observed in the X-ray absorption edge region (Figure 1); one sample of each set exhibited an edge with decreased peak intensity and a shift of the bottom portion of the edge to lower energy. After complete XAS analysis (vide infra), the identities of the samples were revealed and confirmed that this sample in each set was the IPNS·ACV complex. All the differences discussed below were consistently observed in both data sets; spectra are shown for set B only. In addition to the edge differences mentioned above, the data for the IPNS·ACV complex exhibit an increase in the intensity of the 1s → 3d transition at ~7112 eV (Figure 1). The fitting procedure described in the Experimental Procedures resulted in an integrated intensity of this peak of 0.08 eV for IPNS and 0.12 eV for the IPNS·ACV complex. The fit to the overall edge data for the latter sample was improved significantly when a second Gaussian was included, centered at ~7118 eV, which then accounted for a portion of the shift to lower energy of the IPNS·ACV edge.

The analysis of Fe EXAFS data for IPNS and the IPNS·ACV complex are shown in Figures 2 and 3, respectively. Slight but significant differences in the raw EXAFS data (Figures 2a and 3a) are observed, particularly in the reduction in EXAFS amplitude at both ends of the k-range for the IPNS·ACV complex, as well as a change in shape of the features at k = 3–4 Å^{-1}. The EXAFS amplitude reduction for the IPNS·ACV complex is also reflected in the Fourier transform (cf. Figures 2c and 3c). Curve-fitting simulations of the filtered EXAFS data and the corresponding Fourier transforms are compared with the observed data for both samples in Figures 2 and 3, and the results for both sets of sample pairs summarized in Table II. Fits including either 6 Fe–(N,O) or shells of 5 Fe–(N,O) and 1 Fe–S were performed on each of the four data sets.[2] For both substrate-free IPNS samples, the EXAFS data were adequately fit with a single shell of 6 Fe–(N,O); substituting one of the 6 Fe–(N,O)

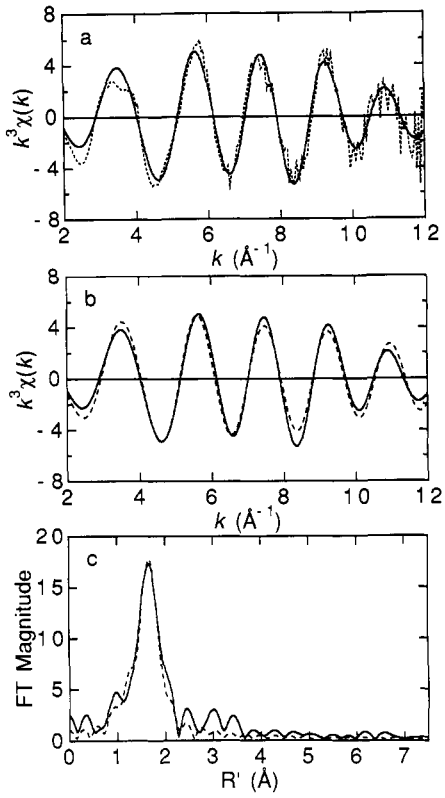

FIGURE 2: Fe EXAFS of IPNS, sample set B. (a) Raw EXAFS (dotted line) and first-shell Fourier filter (solid line). The Fourier transform in (c) was filtered from $R' = 0.6$ to 2.3 Å (with Gaussian shaping function of 0.1-Å width) to yield the filtered data. (b) First-shell Fourier filter (solid line) and best-fit simulation (dashed line) using the metric parameters given in Table II, fit 2E. (c) Fourier transform of raw EXAFS data in (a) (solid line) (k = 2.0–12.0 Å^{-1}, k^3 weighting) and Fourier transform of best-fit simulation of first shell in (b) (dashed line).

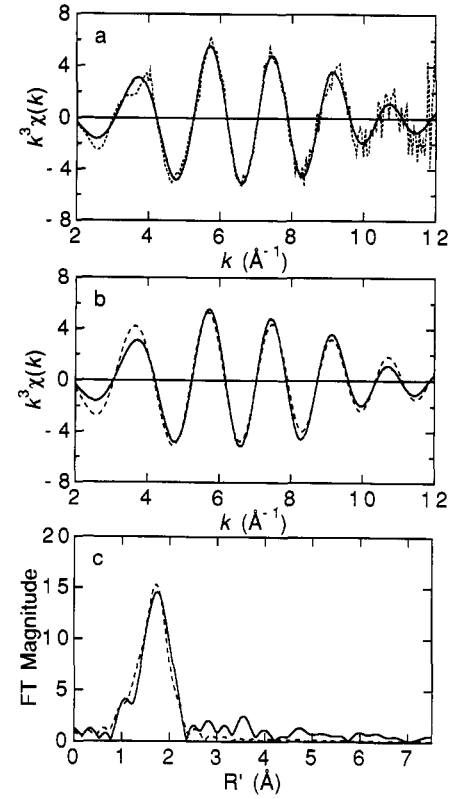

FIGURE 3: Fe EXAFS of the IPNS·ACV complex, sample set B. (a) Raw EXAFS (dotted line) and first-shell Fourier filter (solid line). The Fourier transform in (c) was filtered from $R' = 0.8$ to 2.3 Å (with Gaussian shaping function of 0.1-Å width) to yield the filtered data. (b) First-shell Fourier filter (solid line) and best-fit simulation (dashed line) using the metric parameters given in Table II, fit 2H. (c) Fourier transform of raw EXAFS data in (a) (solid line) (k = 2.0–12.0 Å^{-1}, k^3 weighting) and Fourier transform of best-fit simulation of first shell in (b) (dashed line).

Table II: Curve-Fitting Results for IPNS Samples[a]

sample	fit	shell	N_s	R_{as} (Å)	σ_{as}^2 (Å^2)	f'[b]
free IPNS (set A)	2A	Fe–N	(6)[c]	2.16	0.0042	0.054
	2B	Fe–N	(5)	2.15	0.0031	0.064
		Fe–S	(1)	2.81[d]	0.0537	
IPNS + ACV (set A)	2C	Fe–N	(6)	2.15	0.0057	0.086
	2D	Fe–N	(5)	2.15	0.0076	0.032
		Fe–S	(1)	2.33	0.0039	
free IPNS (set B)	2E	Fe–N	(6)	2.15	0.0035	0.053
	2F	Fe–N	(5)	2.16	0.0031	0.056
		Fe–S	(1)	2.31	0.0100	
IPNS + ACV (set B)	2G	Fe–N	(6)	2.15	0.0050	0.110
	2H	Fe–N	(5)	2.14	0.0064	0.049
		Fe–S	(1)	2.35	0.0016	

[a] N_s is the number of scatterers per iron; R_{as} is the iron–scatterer distance; σ_{as}^2 is a mean square deviation in R_{as}. [b] f' is a goodness-of-fit statistic normalized to the overall magnitude of the $k^3\chi(k)$ data:

$$f' = \frac{\{\sum[k^3(\chi_{obsd}(i) - \chi_{calc}(i))]^2/N\}^{1/2}}{(k^3\chi)_{max} - (k^3\chi)_{min}}$$

where N is the number of data points. [c] Numbers in parentheses were not varied during optimization. [d] Underlined values are chemically and physically unreasonable.

with a second shell of Fe–S yielded no improvement in the fit or a physically unreasonable Fe–S distance and Debye-Waller σ_{as}^2 (Table II, fits 2B and 2F). In contrast, substituting 1 of the 6 Fe–(N,O) with an Fe–S shell was required for a good fit to the IPNS·ACV EXAFS data (Table II, fits 2D and 2H). Improvement upon addition of Fe–S was significantly beyond that expected simply from the larger number of variable parameters.[3] Chemically reasonable Fe–(N,O) distances of 2.15 Å and Fe–S distances of 2.34 Å were obtained in the best fits for both IPNS·ACV data sets. No improvement in any of the fits resulted from splitting the Fe–(N,O) shell into short (~2.10-Å) and long (~2.20-Å) components.[4]

The peaks in the $R' \approx 2.3$–3.7 Å range of the Fourier transforms of both samples (Figures 2c and 3c) most likely result from outer-shell C atoms of side chains of protein-derived Fe ligands. The previous suggestion of histidyl imidazole coordination (Ming et al., 1991) prompted us to use a multiple-scattering analysis (with EXCURV86, see Experimental Procedures) to estimate the expected outer-shell contribution from n imidazoles (n = 1, 2, 3, ...). Assuming that imidazole ligands are responsible for all outer-shell scattering, we estimate that the outer-shell contributions of the FT of the Fe EXAFS of both IPNS and IPNS·ACV samples can be ac-

[3] As discussed by Lee and co-workers (Lee et al., 1981), a modified goodness-of-fit parameter, f'', that takes into account extra degrees of freedom in fits with more variable parameters can be defined as $f'' = f'/N_{fit}$, where $N_{fit} = 2\Delta k\Delta R/\pi - N_{par}$, and N_{par} is the number of variable parameters, Δk is the k-range of data used in the fit, and ΔR is the R-range of the Fourier filter window. For example, for the IPNS + ACV sample from set B (Table II), Δk = 10.0 Å^{-1} and ΔR = 1.5 Å. N_{par} is 2 (R_{as} and σ_{as}^2 for one shell) for fit 2G and 4 for fit 2H, yielding f'' = 0.015 for fit 2G and f'' = 0.009 for fit 2H. A similar improvement is seen for fit 2D (f'' = 0.005) over 2C (f'' = 0.010).

[4] A recent survey of bond distances for structurally characterized high-spin Fe^{2+} complexes suggests that Fe–O distances range from about 2.06 Å (Borovik et al., 1990; Rardin et al., 1990; Rakotonandrasana et al., 1991) to 2.19 Å (Martinez-Lorente et al., 1991; Tolman et al., 1991), whereas Fe–N(imidazole) distances range from about 2.12 Å (Rardin et al., 1990; Tolman et al., 1991) to 2.21 Å (Miller et al., 1989).

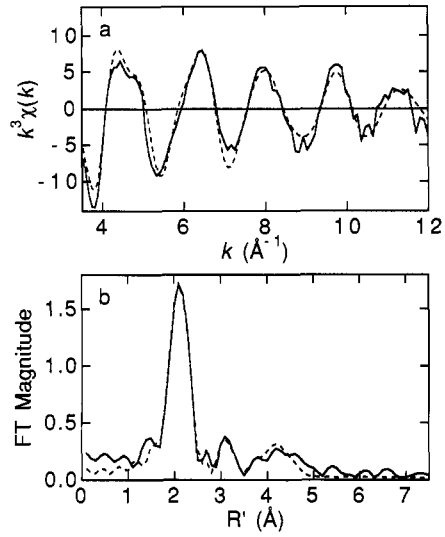

FIGURE 4: Fe EXAFS of IPNS, sample set B, with EXCURV86 simulations. (a) Raw EXAFS (solid line) and best simulation including imidazole rings with multiple scattering (dotted line). (b) Fe–N phase-corrected Fourier transforms of raw EXAFS in (a) (solid line) and of simulation from (a) (dashed line). The simulation used 3 Fe–N scatterers at 2.14 Å (σ_{as}^2 = 0.0045 Å^2) and 3 Fe–imidazole units with Fe–N_1 distances of 2.14 Å (σ_{as}^2 = 0.0045 Å^2), Fe–C_2/–C_5 distances of 3.10/3.11 Å (σ_{as}^2 = 0.0090 Å^2), and Fe–N_3/–C_4 distances of 4.30/4.35 Å (σ_{as}^2 = 0.0150 Å^2). Fe–N_1–C_2 and Fe–N_1–C_5 angles were set to 130° and −125°, respectively, and Fe–N_1–C_3 and Fe–N_1–C_4 angles were set to 165° and −160°, respectively. The amplitude reduction factor (AFAC) was set to 0.9, and k values in (a) have been corrected for the optimized ΔE_0 of 32.2 eV (i.e., these are the values that would result if E_0 of 7097.8 eV were used to calculate k).

counted for with two or three imidazole ligands. An EXCURV86 fit of the IPNS Fe EXAFS assuming three imidazoles and three (N,O)-type ligands contributing only first-shell single scattering is shown in Figure 4. The upper limit of n cannot be firmly established owing to a lack of independent knowledge of possible disorder in the hypothetical set of imidazole ligands. However, the outer-shell FT peaks in Figures 2c and 4b are significantly smaller than those observed in [Cu(imidazole)$_4$]$^{2+}$ (Co et al., 1981), for example.

DISCUSSION

The changes observed in the X-ray absorption edge region (Figure 1) upon ACV binding (reduction of the edge height and a shift to lower energy) are reminiscent of the changes observed upon binding sulfide to the Cu^{2+} site of bovine plasma amine oxidase (Scott et al., 1988) and binding of 2-mercaptoethanol to the Ni^{2+} site of jack bean urease (Clark et al., 1990). All of these changes follow the expected behavior for an increase in covalency of the metal site due to an increase in sulfur ligation (Scott et al., 1986; Eidsness et al., 1988). These observations are in agreement with the results of previous EPR and Mössbauer studies (Chen et al., 1989). The integrated intensity of the 1s → 3d peak at ~7112 eV (Figure 1) was 0.08 eV for the IPNS sample, reflecting a centrosymmetric six-coordinate (octahedral) site (Roe et al., 1984). The edge shape for the free enzyme is similar to that observed for octahedral coordination by (N,O)-containing ligands (Eidsness et al., 1988). Upon ACV binding, the 1s → 3d peak intensity increases to 0.12 eV, placing this site's symmetry between a group of six-coordinate and a group of five-coordinate iron complexes investigated by Roe et al. (1984). The extra transition giving rise to the low-energy shoulder (~7118 eV) in the IPNS·ACV edge spectrum (Figure 1) may represent a shift to lower energy of the "1s → $4p_z$" transition as is also observed in some five-coordinate Ni^{2+} complexes (Eidsness et al., 1988; Colpas et al., 1991). ACV binding may result in a five-coordinate iron center in IPNS, but the presence of one long bond in a six-coordinate site might also explain these EXAFS observations. Furthermore, coordination numbers cannot be determined by EXAFS with sufficient accuracy to distinguish five- and six-coordination (Scott, 1985); the EXAFS analysis for IPNS·ACV assumed overall six-coordination.

Based on a variety of spectroscopic data, a model for the IPNS Fe^{2+} center was formulated to be six-coordinate including two or three histidines, one aspartic acid, and solvent molecules (Ming et al. 1990, 1991; Jiang et al., 1991). Both the coordination number and coordinating atom types of this model are consistent with the Fe EXAFS data presented herein. The average Fe–(N,O) distance of 2.15 ± 0.02 Å is at the low end of the range expected for Fe–N distances (~2.12–2.21 Å)[4] of high-spin Fe^{2+} complexes. Since the Fe–O distances for such complexes range from ~2.06 to 2.19 Å,[4] a mixture of Fe–N and Fe–O distances is consistent with the average distance we observe. Previously, similar average Fe–(N,O) distances were also found by EXAFS analyses of the non-heme Fe^{2+} site in bacterial photosynthetic reaction centers, which consist of four imidazole and one bidentate carboxyl ligands (Bunker et al., 1982; Eisenberger et al., 1982; Allen et al., 1987). Our multiple-scattering analysis is best explained with two or three histidine imidazole ligands although we cannot exactly simulate the FT magnitude near 4.7 Å in Figure 4b. Although our EXAFS analysis cannot rigorously exclude the presence of a tyrosyl phenolate, we have previously argued against its involvement on the basis of other spectroscopic data (Chen et al., 1989; Orville et al., 1992).

With (N,O)-containing ligands participating in predominately ionic interactions, the iron center in IPNS probably displays a relatively high (Fe^{3+}/Fe^{2+}) reduction potential[5] and is therefore likely to be relatively inert to O_2. Substrate binding through the ACV cysteinyl thiolate would lower this reduction potential by increasing the electron density at Fe, thus activating the site for O_2 reduction [for further discussion, see following paper (Orville et al., 1992)]. This could contribute to a driving force for the otherwise energetically prohibitive removal of unactivated hydrogen atoms from the substrate.

A number of spectral changes are consistent with the iron center becoming more covalent upon ACV binding (Chen et al., 1989; Orville et al., 1992; Ming et al., 1990). These have been thought to arise from ACV binding to Fe^{2+} via its thiolate, but an alternative explanation based on tyrosine phenolate coordination upon substrate binding prompted this XAS study. The large difference in atomic mass between sulfur and oxygen makes EXAFS a good technique for distinguishing these alternatives. The data presented herein provide direct evidence for the formation of an Fe–S interaction in the IPNS·ACV complex. Two independent pairs of samples have both shown the requirement for a 2.34-Å Fe–S interaction only after addition of ACV (Table II). This is also within 0.01 Å of the Fe–S bond distances for several thiolate-containing high-spin ferrous heme systems including P-450-CAM and chloroperoxidase (Andersson & Dawson, 1990). Thiolate ligation in IPNS may play the same role in oxygen activation as it does in these heme-containing enzymes.

The origin of the Fe–S interaction observed in the

[5] The (Fe^{3+}/Fe^{2+}) reduction potential of the Fe(carboxylate)(histidine)$_4$ active site of lipoxygenase is estimated as +0.6 V, NHE (Nelson, 1988), and that for the Fe(carboxylate)(histidine)$_3$ active site of Fe-superoxide dismutase has been determined as +0.26 V, NHE (Barrette et al., 1983).

IPNS·ACV complex has not yet been addressed. The most reasonable source is a thiolate sulfur from ACV, but IPNS contains two cysteinyl thiolates that could serve as endogenous Fe^{2+} ligands. In theory, this issue could be resolved by similar EXAFS investigations of genetically engineered variant proteins completely devoid of cysteinyl residues (Kriauciunas et al., 1991). Unfortunately, as is shown in the following paper (Orville et al., 1992), the K_d of ACV for that mutant is ~106 mM, requiring about 1 M tripeptide to achieve 90% formation of the IPNS·ACV complex. The solubility of ACV alone would preclude the XAS studies. However, almost identical Mössbauer, EPR, and optical parameters have been observed for the unaltered IPNS and its mutant devoid of endogenous cysteines as well as for their respective ACV, NO, and ACV + NO complexes. In the mutant complexes, the cysteine of ACV is the only possible thiolate donor to the Fe^{2+} site (Orville et al., 1992). Although the EXAFS data cannot be used to exclude completely the possibility that a methionine thioether coordinates to Fe^{2+} upon ACV binding, the increase in covalency and the existence of ligand-to-iron charge-transfer transition strongly argue against it. Therefore, all data available to date are completely consistent with ACV binding to the Fe^{2+} site through its thiolate sulfur.

ACKNOWLEDGMENTS

The XAS experiments were performed at NSLS, Brookhaven National Laboratory, which is supported by the U.S. Department of Energy, Division of Materials Sciences and Division of Chemical Sciences, and at SSRL, which is operated by the U.S. Department of Energy, Division of Chemical Sciences. The SSRL Biotechnology Program is supported by the NIH, Biomedical Resource Technology Program, Division of Research Resources. We are grateful to Dr. John D. Lipscomb for critical reading of the manuscript.

REFERENCES

Allen, J. P., Feher, G., Yeates, T. O., Komiya, H., & Rees, D., C. (1987) *Proc. Natl. Acad. Sci. U.S.A. 84*, 6162–6166.

Andersson, L. A., & Dawson, J. H. (1990) *Struct. Bond. 74*, 1–40.

Baldwin, J. E., & Abraham, E. P. (1988) *Nat. Prod. Rep. 5*, 129–145.

Barrette, W. C., Sawyer, D. T., Fee, J. A., & Asada, K. (1983) *Biochemistry 22*, 624–627.

Borovik, A. S., Hendrich, M. P., Holman, T. R., Münck, E., Papaefthymiou, V., & Que, L., Jr. (1990) *J. Am. Chem. Soc. 112*, 6031–6038.

Bunker, G., Stern, E. A., Blankenship, R. E., & Parson, W. W. (1982) *Biophys. J. 37*, 539–551.

Chan, S. I., Witt, S. N., & Blair, D. F. (1988) *Chem. Scr. 28A*, 51–56.

Chen, V. J., Orville, A. M., Harpel, M. R., Frolik, C. A., Surerus, K. K., Münck, E., & Lipscomb, J. D. (1989) *J. Biol. Chem. 264*, 21677–21681.

Clark, P. A., Wilcox, D. E., & Scott, R. A. (1990) *Inorg. Chem. 29*, 579–581.

Co, M. S., Scott, R. A., & Hodgson, K. O. (1981) *J. Am. Chem. Soc. 103*, 986–988.

Colpas, G. J., Maroney, M. J., Bagyinka, C., Kumar, M., Willis, W. S., Suib, S. L., Baidya, N., & Mascharak, P. K. (1991) *Inorg. Chem. 30*, 920–928.

Cramer, S. P., Tench, O., Yocum, M., & George, G. N. (1988) *Nucl. Instrum. Methods Phys. Res., Sect. A A266*, 586–591.

Eidsness, M. K., Sullivan, R. J., & Scott, R. A. (1988) in *Bioinorganic Chemistry of Nickel*, (Lancaster, J. R., Ed.) pp 73–91, VCH, Deerfield Beach, FL.

Eisenberger, P., Okamura, M. Y., & Feher, G. (1982) *Biophys. J. 37*, 523–538.

Ingraham, L. L., & Meyer, D. L. (1985) in *Biochemistry of Dioxygen*, pp 139–246, Plenum Publishing Co., New York.

Jiang, F., Peisach, J., Ming, L.-J., Que, L., Jr., & Chen, V. J. (1991) *Biochemistry 30*, 11437–11445.

Kriauciunas, A., Frolik, C. A., Hassell, T. C., Skatrud, P. L., Johnson, M. G., Holbrook, N. L., & Chen. V. J. (1991) *J. Biol. Chem. 266*, 11779–11788.

Lee, P. A., Citrin, P. H., Eisenberger, P., & Kincaid, B. M. (1981) *Rev. Mod. Phys. 53*, 769–806.

Martinez-Lorente, M.-A., Tuchagues, J.-P., Pêtrouléas, V., Savariault, J.-M., Poinsot, R., & Drillon, M. (1991) *Inorg. Chem. 30*, 3587–3589.

Miller, L. L., Jacobson, R. A., Chen, Y.-S., & Kurtz, D. M. (1989) *Acta Crystallogr. C45*, 527–529.

Ming, L.-J., Que, L., Jr., Kriauciunas, A., Frolik, C. A., & Chen, V. J. (1990) *Inorg. Chem. 29*, 1111–1112.

Ming, L.-J., Que, L., Jr., Kriauciunas, A., Frolik, C. A., & Chen, V. J. (1991) *Biochemistry 30*, 11653–11659.

Nelson, M. J. (1988) *Biochemistry 27*, 4273–4278.

Orville, A. M., Chen, V. J., Kriauciunas, A., Harpel, M. R., Fox, B. G., Münck, E., & Lipscomb, J. D. (1992) *Biochemistry* (following paper in this issue).

Rakotonandrasana, A., Bionnard, D., Savariault, J.-M., & Tuchagues, J.-P. (1991) *Inorg. Chim. Acta 180*, 19–31.

Rardin, R. L., Bino, A., Poganiuch, P., Tolman, W. B., Liu, S., & Lippard, S. J. (1990) *Angew. Chem., Intl. Ed. Engl. 29*, 812–814.

Rehr, J. J., Leon, J. M. d., Zabinsky, S. I., & Albers, R. C. (1991) *J. Am. Chem. Soc. 113*, 5135–5140.

Roe, A. L., Schneider, D. J., Mayer, R. J., Pyrz, J. W., Widom, J., & Que, L., Jr. (1984) *J. Am. Chem. Soc. 106*, 1676–1681.

Scott, R. A. (1985) *Methods Enzymol. 117*, 414–459.

Scott, R. A., Schwartz, J. R., & Cramer, S. P. (1986) *Biochemistry 25*, 5546–5555.

Scott, R. A., Cotê, C. E., & Dooley, D. M. (1988) *Inorg. Chem. 27*, 3859–3861.

Strange, R. W., Blackburn, N. J., Knowles, P. F., & Harris, S. S. (1987) *J. Am. Chem. Soc. 109*, 7157–7162.

Tolman, W. B., Liu, S., Bentsen, J. G., & Lippard, S. J. (1991) *J. Am. Chem. Soc. 113*, 152–164.

White, R. L., John, E.-M. M., Baldwin, J. E., & Abraham, E. P. (1982) *Biochem. J. 203*, 791–793.